Effects of geometrical and thermophysical parameters on heat transfer measurements in small diameter channels

Bruno Agostini, André Bontemps, Bernard Thonon

Effects of Geometrical and Thermophysical Parameters on Heat Transfer Measurements in Small-Diameter Channels

BRUNO AGOSTINI
Laboratory of Heat and Mass Transfer, Ecole Polytechnique Fédérale de Lausanne, Switzerland

ANDRÉ BONTEMPS
LEGI/GRETh, Université Joseph Fourier, Grenoble, France, and CEA-GRETh, Grenoble, France

BERNARD THONON
CEA-GRETh, Grenoble, France

An experimental investigation of the liquid flow friction factor and heat transfer coefficient in small diameter channels is presented. Rectangular and circular mini-channels with hydraulic diameters from 0.77 to 2.01 mm were used. Literature in the 1990s showed scattered experimental results and concluded that new physical phenomena in mini-channels could occur. However, the present experimental results show that three main causes can explain how different results were obtained in mini-channels compared to macro-tubes: uncertainties on the channel dimensions, inlet and outlet singular pressure losses, and longitudinal heat conduction. When these elements are taken into account, good agreement is found with standard correlations or theories.

INTRODUCTION

In recent years, an interest in heat transfer at small scales has led to an increase in their reference in publications. In particular, mini-channels are of high interest to the industry due to the possibility of manufacturing efficient compact heat exchangers. Indeed, mini-channel heat exchangers with a hydraulic diameter of about 1 mm achieve higher heat transfer coefficients and thermal efficiency and a lower fluid charge, all of which allow for space savings and lower costs.

Table 1 summarizes the experimental conditions of previous studies on mini-channels. In the sixth column, the critical Reynolds numbers from laminar to turbulent flow estimated by other authors are reported. Figure 1 shows the spectrum of ratios between friction factors and Nusselt numbers for mini-channels (reported in Table 1) and conventional correlations for macro-tubes, for both laminar and turbulent regimes. It appears that in the early 1990s, results found in the literature are not consistent either with macro-tubes correlations or among themselves. On the contrary, the most recent literature from Agostini et al. [1] and Owhaib and Palm [2] shows a convergence of experimental data in mini-channels toward those correlations. Accordingly, in a recent literature review on the size effect on microscale single-phase flow and heat transfer, Guo and Li [3] emphasized that "discrepancies between experimental results for the friction factor and the Nusselt number and their standard values due to the measurement errors might be misunderstood as being caused by novel phenomena at microscale." According to Table 1, results found in the literature on heat transfer in mini-channels are often contradictory and difficult to compare due to differing operating conditions between studies. Some authors show experimental results in good agreement with traditional results in

B. Agostini received support from ADEME (French Agency for Environment and Energy Management) and CEA (French Atomic Energy Commission) for this project. The authors would like to acknowledge the technical input of S. Arnaud.

Address correspondence to Dr. Bruno Agostini, Laboratory of Heat and Mass Transfer (LTCM), Faculty of Engineering Science, Swiss Federal Institute of Technology of Lausanne (EPFL), CH-1015 Lausanne, Switzerland. E-mail: bruno.agostini@epfl.ch

Table 1 Summary of experimental conditions of previous studies

Year	Author	Fluid	Geometry	D_h(mm)	Re	Re_{cr}
1991	Choi and Barron [15]	Nitrogen	Rectangular	0.003–0.081	30–3000	≈ 2000
1994	Peng et al. [18]	Water	Rectangular	0.133–0.367	50–4000	200–700
1994	Wang and Peng [19]	Water	Rectangular	0.311–0.747	80–3000	1000–1500
1995	Peng and Peterson [20]	Water	Rectangular	0.311–0.646	200–2500	400–1000
1996	Peng and Peterson [21]	Water	Rectangular	0.133–0.367	450–4000	70–400
1996	Yang and Webb [22]	R12	Rectangular	1.56–3.25	2500–23000	—
1998	Adams et al. [14]	Water	Circular	0.76–1.09	2600–23000	—
1999	Harms et al. [23]	Water	Rectangular	0.4–1.92	173–12900	≈500
1999	Mala and Li [24]	Water	Rectangular	0.05–0.254	100–2000	≈500
1999	Yan and Lin [25]	R134a	Circular	2.00	400–10000	≈2000
2001	Garimella et al. [16]	Glycol	Rectangular	1.74–3.02	118–10671	800–2000
2001	Hegab et al. [26]	R134a	Rectangular	0.112–0.210	1200–13200	2000–4000
2002	Ohwaib and Palm [2]	R134a	Circular	0.8–1.7	1000–16000	—
2002	Celata et al. [27]	R114	Circular	0.130	100–8000	1880–2480
2002	Agostini et al. [28]	R134a	Rectangular	0.77–1.17	320–12691	≈2000
2003	Agostini et al. [1]	R134a	Rectangular	2.01	242–7356	≈2000

macro-tubes, while in a number of cases, new physical processes or phenomena are supposed to be preponderant at small scales to explain significant deviations. However, phenomena like the Electrical Double Layer, the viscous dissipation, or the breaking of the continuous medium approximation for gases should not occur over about ten μm. It is also reported that vapor trapped in the wall bumps or the effect of tube roughness creating turbulent wakes may have an increased influence in mini-channels. This study presents experimental friction factors and heat transfer coefficients obtained in four mini-channels of varied size and geometry, using refrigerant R134a liquid flow. Experimental results in mini-channels agree with those obtained in macro-tubes, provided that experimental conditions are tightly controlled, that measurements are carried out with increased care, and that the usual hypotheses in the data analysis are still valid. Three error sources of importance at small scales were identified: large uncertainties on the channel dimensions, singular pressure losses in manifolds, and longitudinal heat conduction in the tube walls in the laminar regime.

EXPERIMENTAL DEVICE

The test loop (shown in Figure 2) includes a liquid pump (10–100 l/h) and a glycol-water mixture circuit for heat evacuation. The test section, shown in Figure 3, consists of industrial flat tubes made of extruded aluminium and composed of numerous parallel rectangular channels or of independent parallel tubes for the circular geometry. Table 2 gathers the characteristics of all the tested geometries. The inlet and outlet manifolds are 10 mm-diameter tubes at 90 degrees. The manifold diameter is between five and thirteen times greater than the channel hydraulic diameter to limit the fluid distribution effects. The whole

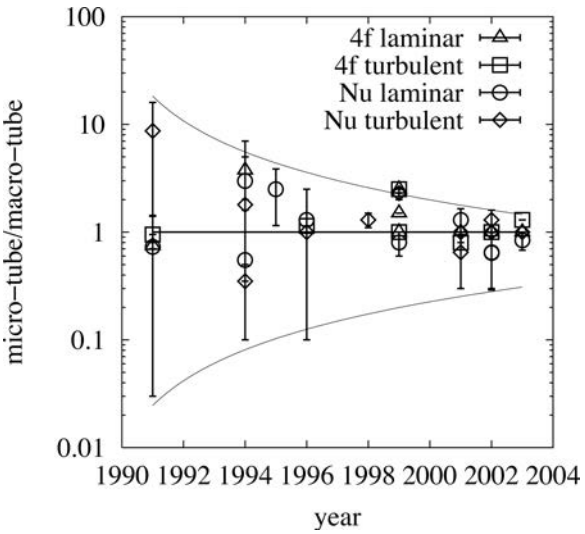

Figure 1 Convergence toward macro-tubes correlations.

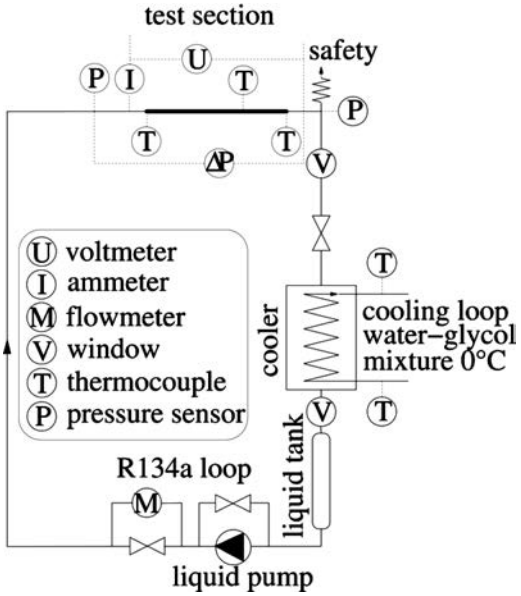

Figure 2 Test loop.

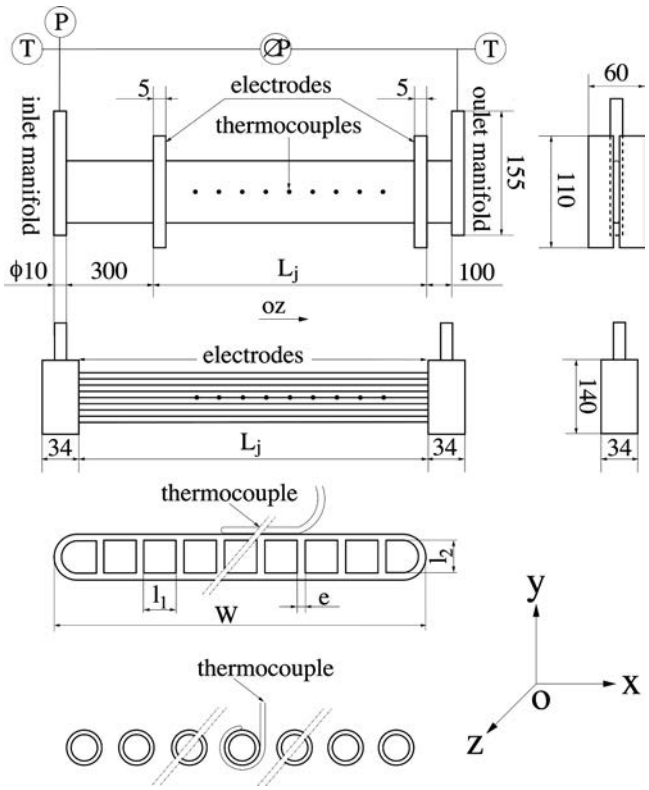

Figure 3 Test section, for rectangular and circular channels, dimensions in mm.

test section is thermally insulated with 40 mm-thick wrapping foam. For heat transfer measurements, the length L_j of the tube was heated using Joule effect by passing an electric current (up to 2800 A) from two brased electrodes through the tube wall. Experimental conditions are summarized in Table 3.

Figure 3 shows the test sections and instrumentation. It is worth noting that in the case of the circular channels, the test section was built with independent mini-tubes, and the electrodes were manufactured with the manifold on the same aluminium piece. Wall temperatures $T_{w,k}$ $(0 < k < 9)$ on the tube external surface were measured with 0.5 mm-diameter calibrated type E thermocouples. Fluid inlet and outlet mixed mean temperatures (respectively, $T_{f,in}$ and $T_{f,out}$) were measured with 1 mm-diameter calibrated type K thermocouples in a T junction to ensure mixing. Calibration was carried out every five K between 268 and 333 K with a Rosemount 162-CE platinum thermometer. The thermocouples used for wall temperature measurements were equally spaced and fixed on the tube surface. The fluid inlet pressure was measured with calibrated Rosemount type II absolute pressure sensors. Three Kent-Deltapi K differential pressure sensors calibrated from 0 to 7.6, 40.5, and 182.2 kPa measured the pressure loss through the test section. A Rosemount Micromotion coriolis flowmeter was used to measure the mass flux of R134a downstream of the pump. The heating voltage V and current I (via a shunt) were measured directly via a HP 3421A multiplexer.

Table 2 Tested geometries

Tube	1	2	3	4
D_h (mm)	2.01 ± 3 %	1.44 ± 1 %	1.17 ± 4 %	0.77 ± 7 %
Shape	Rectangular	Circular	Square	Square
l_1 (mm)	3.28 ± 0.02	—	1.11 ± 0.02	0.73 ± 0.01
l_2 (mm)	1.47 ± 0.02	—	1.22 ± 0.01	0.72 ± 0.01
e (mm)	0.35	0.29	0.3	0.25
N	11	24, 12	31	18
L_j (mm)	690 ± 2.5	1060 ± 0.4	688 ± 5	695 ± 2.5
A_{al} (mm^2)	51 ± 2.5	19 ± 0.4	52 ± 1	13 ± 0.5

Table 3 Operating conditions

	Friction Factor	
	Value	Error
Re	142–8,093	±3–8%
T_w, T_f (K)	273–281	±0.1K
$\Delta T_{sub,in}$ (K)	≈ 40	—
p_{in} (kPa)	≈ 1700	—
Δp (kPa)	0.3–172.2	±0.3–25%
$4f$	0.04–0.45	±7–31%
Flow	Horizontal	
Heat transfer coefficient		
Re	277–13,335	±3–8%
$\dot{q}$ (kW/m^2)	0.84–22	±3%
T_w, T_f (K)	270–332	±0.1–1.4 K
$\Delta T_{sub,in}$ (K)	≈ 70	—
p_{in} (kPa)	≈ 2000	—
Pr	3.2–4	0.05–0.70%
Nu	0.9–91	±3–28%
Flow	Ascendant	

The heat flux was varied for every mass flow rate in order to keep the fluid temperature rise between 20 and 40 K. Steady state values were monitored using the Hewlett Packard 3421A with a 30-minute time lapse between each mass flow rate or heat flux change. Averaging occurred after every twenty values, and the standard deviation was used to calculate the uncertainties according to the Kline & McClintock [4] and Moffat [5, 6] methods. The uncertainty on temperature measurements was estimated to be ±0.1 K. The thermocouples' locations were measured with a calliper rule, and the corresponding uncertainty, ±0.5 mm, was taken into account in the Kline & McClintock method. The other uncertainties are reported in Tables 2 and 3. The total electrical power dissipated in the test section was calculated as the product of voltage and current. The variation of R134a thermophysical properties with temperature was calculated with the REFPROP 6.01 software from the NIST Standard Reference Database 23.

Non-uniform flow distribution can occur in multi-channels systems. In order to avoid this effect, the engineering rule that the manifolds diameter should be at least five times higher than the channel hydraulic diameter to equalize the fluid distribution was used. This does not ensure that non-uniform distribution is totally suppressed, but it should reduce it to within acceptable limits. However, even if non-uniform distribution

occurs, it will not affect the inlet and outlet measurements, which are performed out of the manifolds. The local temperature measurements should also not be affected because of the averaging of wall temperatures across the N channels due to the aluminium's very high thermal conductivity.

THE DRAMATIC ROLE OF THE GEOMETRICAL UNCERTAINTIES

A classical uncertainty analysis in the case of a nearly square channel, taking only into account errors on dimensions, immediately demonstrates the influence of small geometrical uncertainties on $4f$ and Nu. If l_1 is the length of a channel side, it is known that

$$4f = \Delta p_f \cdot \frac{D_h}{L} \cdot \frac{2\rho_l \cdot S_f^2}{\dot{M}^2}, \tag{1}$$

yielding

$$4f = \frac{\Delta p_f}{L} \cdot \frac{2l_1 \cdot l_2}{l_1 + l_2} \cdot \frac{2\rho_l (l_1 \cdot l_2)^2 \cdot N^2}{\dot{M}^2}, \tag{2}$$

so that

$$\frac{\Delta 4f}{4f} = 3\frac{\Delta l_1}{l_1} + 3\frac{\Delta l_2}{l_2} + \frac{\Delta(l_1 + l_2)}{l_1 + l_2}. \tag{3}$$

If $l_1 = l_2$, then

$$\frac{\Delta 4f}{4f} \approx 7\frac{\Delta l_1}{l_1}. \tag{4}$$

The same reasonning leads to

$$\frac{\Delta \mathrm{Nu}}{\mathrm{Nu}} = \frac{V \cdot \mathrm{I}}{k_f \cdot L \cdot (T_w - T_f)} \frac{l_1 \cdot l_2}{(l_1 + l_2)^2} \approx 4\frac{\Delta l_1}{l_1}. \tag{5}$$

As a consequence, an error as low as $\pm 2\%$ on the channels' dimensions leads to uncertainties of $\pm 14\%$ on 4f and $\pm 8\%$ on Nu, for the geometrical part of the uncertainty only. Upon adding the other uncertainties onto pressure or temperature measurements, for instance, the total uncertainty can then very easily reach $\pm 30\%$ in the laminar regime. This obvious remark should be an incentive to determine the dimensions of mini-channels, in particular rectangular channels, with great care.

In order to reach the required degree of accuracy, the determination of the channel dimensions was carried out using scanning electron microscopy on several channels on different sections of tubes, allowing measurements to be done with precision. It is evident from Figure 4, which shows an electron microscopy photograph of the mini-channels, that the knowledge of l_1 and l_2 dimensions is not sufficient to calculate the hydraulic diameter. Indeed the circular corners and the rounded side channels must be taken into account to obtain an accurate value of D_h. Accordingly, the hydraulic diameter was calculated by

$$D_h = \frac{4A_f}{P_f}. \tag{6}$$

A_f and P_f are the total wetted area and perimeter, including the N channels. Both A_f and P_f were determined from several

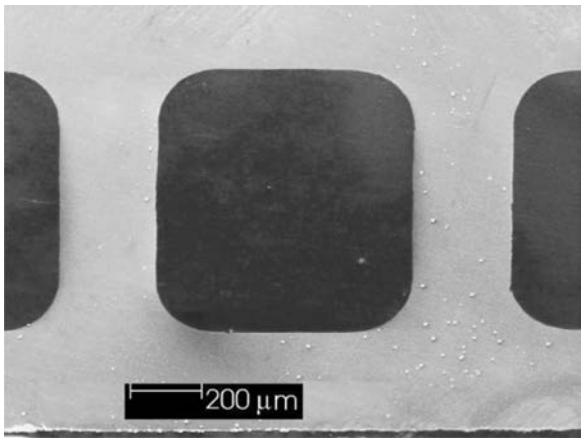

Figure 4 Electron microscopy picture of the 0.77 mm hydraulic diameter mini-channel.

electron microscopy pictures. Several values were averaged and twice the standard deviation (95% confidence level) was taken for the uncertainties. This method ensured that all the geometric features were included. Table 4 shows the difference between the actual hydraulic diameter (Eq. 6) and that calculated from the manufacturer's blueprints, or the dimensions l_1 and l_2. These differences can be important and justify the use of Eq. (6) to calculate D_h.

Furthermore, roughness measurements were carried out on tubes 1, 3, and 4, leading to $R_a/D_h = 3 \times 10^{-4}$, so that these tubes can be treated as smooth tubes.

FRICTION FACTOR AND SINGULAR PRESSURE LOSSES

Pressure loss measurements were performed under adiabatic conditions. The total pressure loss through the test section is:

$$\Delta p = \Delta p_{fr} + \Delta p_{\sin g} \tag{7}$$

with the frictional pressure loss

$$\Delta p_{fr} = \frac{G^2}{2\rho_l} \cdot 4f \cdot \frac{L}{D_h} \tag{8}$$

and the singular pressure loss

$$\Delta p_{\sin g} = \frac{G^2}{2\rho_l} \cdot \xi \tag{9}$$

Since pressure loss measurements were performed with a horizontal configuration, there is no gravitational pressure loss.

Table 4 Comparison of different hydraulic diameters

mm	$4A_f/P_f$	D_h (blueprint)	$2l_1 \cdot l_2/(l_1 + l_2)$
Tube 1	2.01	2.06 (+2%)	2.03 (+1%)
Tube 2	1.44	1.40 (−3%)	—
Tube 3	1.17	1.29 (+10%)	1.16 (−1%)
Tube 4	0.77	0.70 (+9%)	0.72 (−6%)

In parenthesis are the differences with column 2.

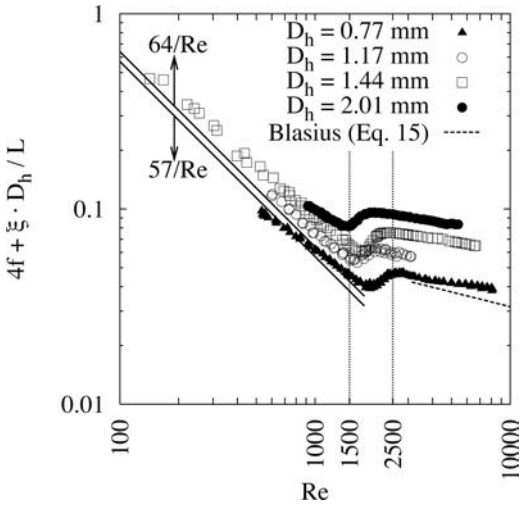

Figure 5 $4f + \xi \cdot D_h/L$ versus Re; uncertainties are in Table 3.

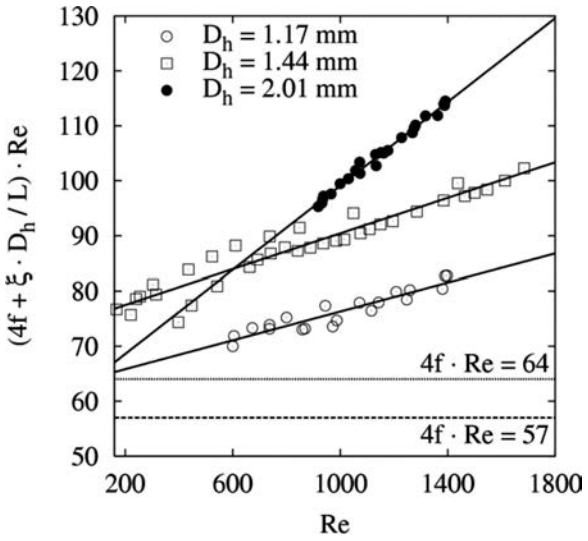

Figure 6 Determination of the singular pressure loss coefficient; uncertainties are in Table 3.

Thus, experimental pressure losses can be expressed under the dimensionless form

$$\frac{2\rho_l \cdot D_h}{G^2 \cdot L} \cdot \Delta p = 4f + \xi \cdot \frac{D_h}{L}. \tag{10}$$

This dimensionless pressure loss is plotted in Figure 5 as a function of the Reynolds number and is compared with the friction factors for rectangular, circular, and square ducts. In the laminar regime, these friction factors are given by the generic relation $4f \cdot \mathrm{Re} = constant$, the constant depending on the geometry; in the turbulent regime, they are given by the Blasius relation. It is apparent from Figure 5 that friction pressure losses cannot account for the experimental ones. The following argument demonstrates that this is due to singular pressure losses.

The frictional pressure loss in the straight part between the pressure sensor and the manifold is about 0.3% of the total pressure loss. This effect is then negligible. In order to assess the singular pressure loss coefficient caused by the T junctions in the manifolds, Eq. (10) multiplied by Re was plotted against the Reynolds number for $140 < \mathrm{Re} < 1\,700$ (see Figure 6). In the laminar regime, the friction factor should not depend on the tube roughness so that the inlet and outlet effects can be isolated in this region. The linearity of the points on Figure 6 indicates that Eq. (10) is equivalent to

$$4f \cdot \mathrm{Re} + \xi \cdot \frac{D_h}{L} \times \mathrm{Re} = b + a \cdot \mathrm{Re}, \tag{11}$$

with a and b being numerical constants. The singular pressure loss coefficient is a function of the manifolds geometry only so that it is independent of Re. Thus, it is possible to identify the right and left hand terms of Eq. (11). Since $\xi \cdot D_h/L$ is constant, this identification necessarily gives

$$4f \cdot \mathrm{Re} = b \quad \text{and} \quad \xi \cdot \frac{D_h}{L} = a. \tag{12}$$

The singular pressure loss coefficient taking into account inlet and outlet effects can be calculated with this method, and the $4f \cdot \mathrm{Re}$ product is found to be constant as expected. Results are gathered in Table 5. Uncertainties are calculated by evaluating Eq. (11) with lower and higher error marks.

The $4f$ factors evaluated with Eq. (10) can now be plotted as functions of Re (see Figure 7), together with the Shah and London [7] correlation for a laminar flow in rectangular channels,

$$4f \cdot \mathrm{Re} = 96(1 - 1.3553 \cdot \gamma + 1.9467 \cdot \gamma^2 - 1.7012 \cdot \gamma^3 + 0.9564 \cdot \gamma^4 - 0.2537 \cdot \gamma^5), \tag{13}$$

the well known Poiseuille law for circular channels,

$$4f \cdot \mathrm{Re} = 64 \tag{14}$$

and the Blasius [8] correlation for turbulent flows,

$$4f = 0.316 \cdot \mathrm{Re}^{-0.25}. \tag{15}$$

The laminar–turbulent transition is clearly visible for $1400 < \mathrm{Re} < 2000$, very close to the accepted value for macrotubes. As highlighted by Tam and Ghajar [9], who studied the effect of the inlet conditions on the laminar-turbulent transition, severe inlet conditions like re-entrant inlets should cause the transition to happen at lower Reynolds numbers than smooth inlets. This effect is indeed observed in the present results. In the laminar regime, the friction factor is in good agreement,

Table 5 Comparison of pressure drop parameters for channels of different hydraulic diameters

	$4f \cdot \mathrm{Re}$		$4f \cdot \mathrm{Re}^{0.25}$			
D_h (mm)	Re < 1800	Eq. (13, 14)	Re > 2000	Eq. (15)	ξ	A_Φ/A_f
2.01	61 ± 8.5	63.8	0.388 ± 0.04	0.316	21 ± 0.5	1.5
1.44	74 ± 12	64	0.434 ± 0.03	0.316	11 ± 3	2.0
1.17	63 ± 13	57	0.329 ± 0.03	0.316	12 ± 6	1.9
0.77	57 ± 11	57	0.347 ± 0.04	0.316	—	7.4

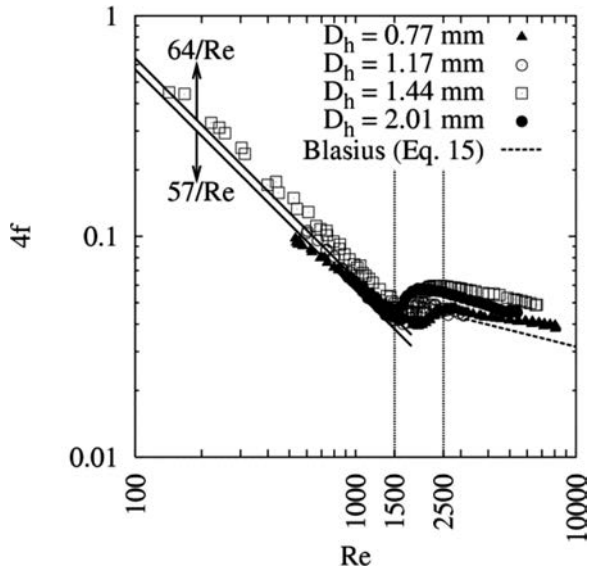

Figure 7 Friction factor versus Reynolds number; uncertainties are in Table 3.

within uncertainties, with Eqs. (13) and (14). In the developing turbulent regime, the friction factor is underpredicted by Eq. (15) for tubes 1 and 2 and within uncertainties for tubes 3 and 4.

Table 3 indicates uncertainties on $4f$ and Re. Finally, results in both the laminar and turbulent regime are in quite good agreement with the results in macro-tubes. The observed maximum deviation is +37% with the Blasius correlation for tube 1, which has a behavior slightly different from the others. This might be due to the relative importance of the side channels because of the reduced number of mini-channels (11) in tube 1.

In the last column of Table 5, the ratio between the manifolds and channels flow areas are reported. Compared to the ξ column, it appears that the ratio A_Φ/A_f is characteristic of the singular pressure loss coefficient, which decreases with increasing A_Φ/A_f. From the data on tube 4, for which uncertainties alone can explain the small deviations from known results, it can be assumed that for $A_\Phi/A_f > 10$, ξ is negligible. This may be taken as a rule of thumb for manifold design.

HEAT TRANSFER COEFFICIENT AND LONGITUDINAL CONDUCTION

The variation of $\mathrm{Pr}^{1/3}$ due to the fluid temperature rise is about 2% so that it cannot explain the observed variations of the Nusselt number. The implicit assumption of one-dimensional conduction, i.e. between the external and internal tube wall only, is the starting point to calculate Nusselt numbers from experimental heat transfer data. Our goal is to show from experimental data analysis that this assumption is frequently wrong in the case of mini-channels for which the wall thickness can be of the same order of magnitude as the hydraulic diameter (e is 30% of D_h for tube 4).

Heating by means of the Joule effect ensures that the volumetric power density is uniform within the aluminium and that the heat flux does not depend on z if heat losses are neglected. However, it cannot be inferred that the peripheral heat flux around a channel is uniform. Some numerical simulations [10] with the FLUENT software proved that as a consequence of the high thermal conductivity of aluminium and the low heat transfer coefficients in the laminar regime, the internal wall temperature is uniform at the periphery of a channel. On the contrary, the heat flux varies and is nearly nil in the corners. If A_x, $\dot{q}_y(x)$, $h(x)$ and A_y, $\dot{q}_x(y)$, $h(y)$ are the heat transfer areas, heat fluxes, heat transfer coefficients parallel to the ox and oy axis, respectively, the average heat transfer coefficients on each wall can be calculated as follows (see Figure 3 for x,y coordinates):

$$h(x) = \frac{\dot{q}_y(x)}{T_w - T_f} \quad \text{and} \quad h(x) = \frac{\dot{q}_x(y)}{T_w - T_f}, \tag{16}$$

and the average peripheral heat transfer coefficient is

$$\bar{h} = \frac{\bar{h}(x) \cdot A_x + \bar{h}(y) \cdot A_y}{A_j} = \frac{\bar{\dot{q}}_y(x) \cdot A_x + \bar{\dot{q}}_x(y) \cdot A_y}{A_j \cdot (T_w - T_f)} \tag{17}$$

$$= \frac{\bar{\dot{q}}}{T_w - T_f}$$

with

$$\bar{\dot{q}} \cdot A_j = \bar{\dot{q}}_y(x) \cdot A_x + \bar{\dot{q}}_x(y) \cdot A_y, \tag{18}$$

as the temperature difference $T_w - T_f$ is constant over the periphery of a channel. As a consequence, the average heat flux, subsequently noted $\dot{q}$,

$$\dot{q} = \frac{V \cdot I}{A_j} = \frac{V \cdot I}{P_f \cdot L_j}. \tag{19}$$

can be used to calculate the average peripheral heat transfer coefficient, which is the relevant parameter.

Let us now assume that only one-dimensional phenomena occur, and let us conduct the classical reasoning to extract Nusselt numbers from measurements. Due to the high thermal conductivity of the aluminium (≈200 W/m K) and the low thickness of the tube walls, the measured temperature ($T_{w,ext}$) is equal to the wall temperature in contact with the fluid ($T_{w,int}$). This can be shown by using classical one-dimensional conduction (see Eq. [20]). Using this equation, the temperature difference is estimated to be less than 0.01 K,

$$T_{w,ext} - T_{w,int} = \frac{\omega \cdot e^2}{k_{al}} + \frac{\dot{q}_{leak} \cdot e}{k_{al}}, \tag{20}$$

where ω is the volumetric power density and $\dot{q}_{leak}$ is the heat leaks density.

The energy balance was checked, and thermal leaks, defined by

$$\dot{Q}_{leak} = \dot{M} \cdot c_{p,l} \cdot (T_{fl,out} - T_{fl,in}) - V \cdot I. \tag{21}$$

were found to be less than 15%, 10%, and 5% of the injected power for 100%, 87%, and 52% of the data points, respectively. Therefore the fluid temperature at z position was calculated via

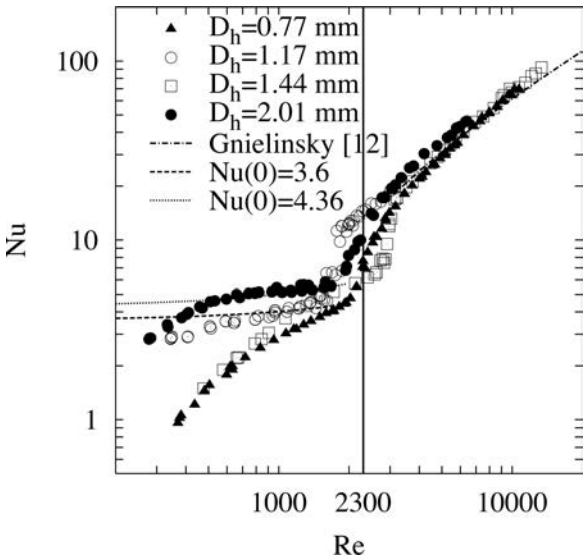

Figure 8 Averaged Nusselt number versus averaged Reynolds number. Nu(0) is the asymptotic theoretical prediction from [7] when Re $\rightarrow$ 0; uncertainties are in Table 3.

an energy balance ($\dot{Q}_{leak} = 0$), giving

$$T_f(z) = T_{f,in} + \frac{V \cdot I}{\dot{M} \cdot c_{p,l} \cdot L_j} \cdot z \tag{22}$$

Two different heat transfer coefficients, a local and an averaged one, were determined. The local heat transfer coefficient and Nusselt numbers are defined as

$$h(z) = \frac{\dot{q}}{T_w(z) - T_f(z)} \quad \text{and} \quad \mathrm{Nu}(z) = \frac{h(z) \cdot D_h}{k_l(z)}. \tag{23}$$

The average Nusselt number is defined as

$$\mathrm{Nu} = \frac{1}{10} \sum_{k=0}^{9} \mathrm{Nu}_k. \tag{24}$$

Accordingly, the local and average Reynolds numbers are

$$\mathrm{Re}(z) = \frac{G \cdot D_h}{\mu_l(z)} \quad \text{and} \quad \mathrm{Re} = \frac{1}{10} \sum_{k=0}^{9} \mathrm{Re}_k. \tag{25}$$

It was verified that mixed convection could not occur. Indeed, according to Ghajar and Tam [11], over the present Reynolds number range with a uniform heat flux condition, the mixed convection should occur for $\mathrm{Gr} \cdot \mathrm{Pr} \cdot D_h/L_j > 330$, while the value for the present experiment was approximately 20. Thus, only forced convection can take place.

In Figure 8, the averaged Nusselt numbers are plotted against the Reynolds number for each tube. In every case, as already observed from the friction factor, the transition from the laminar to the turbulent regime occurs for Re $\approx$ 2000. In the turbulent regime, the global Nusselt number agrees with the Gnielinski [12] correlation, modified to take into account the thermal entry length effect

$$\mathrm{Nu} = \frac{(f/2) \cdot (\mathrm{Re} - 1000) \cdot \mathrm{Re}}{1 + 12.7 \cdot \sqrt{f/2} \cdot (\mathrm{Pr}^{2/3} - 1)} \cdot \left[1 + \left(\frac{D_h}{L_j}\right)^{2/3}\right], \tag{26}$$

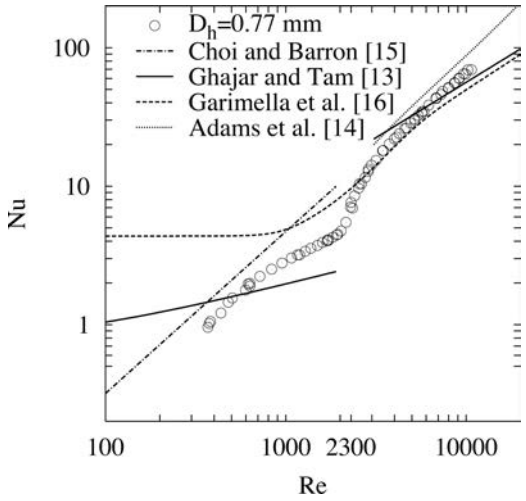

Figure 9 Comparison of averaged Nusselt number versus averaged Reynolds number with some recent correlations (tube 4).

with f calculated using Eq. (15). This correlation is valid for $2300 < \mathrm{Re} < 10^6$ and $0.6 < \mathrm{Pr} < 10^5$.

In Figure 9 the Nusselt numbers obtained with the 0.77mm-hydraulic diameter tube are compared with some recent heat transfer correlations. The Ghajar and Tam [13] correlation was designed to take into account entry effects in macroscale tubes. Adams et al. [14], Choi and Barron [15], and Garimella et al. [16] correlations were obtained with heat transfer data in minichannels, as reported in Table 1. The correlation proposed by Ghajar and Tam [13] for a re-entrant inlet, similar to the present case, is compared to the present results. The prediction is the best of the four tested correlations, in particular in the laminar regime, but the slope of the Nu(Re) curve is still wrong. However, in the turbulent regime, the presented experimental results are still best predicted by the Gnielinski [12] correlation.

If the laminar regime is fully developed, the Nusselt numbers should be constant. Figure 8 shows that this is not the case, and an increase of Nu with Re is observed. As a consequence, the effect of the entry length is first studied. The thermal entry length for constant heat flux heating is given by $L_{th}/D_h = 0.0431 \cdot \mathrm{Re} \cdot \mathrm{Pr}$ [17]. In the present experiment, for $300 < \mathrm{Re} < 2000$ and tube 1, $L_j/D_h = 343$ and $50 < L_{th}/D_h < 320$; thus, the heated and entry lengths are of the same order of magnitude. It is then possible that the flow is not fully developed. As a result, Nu slightly increases with Re in the laminar region. The Shah and London [7] tabulated values for a thermally developing flow are reported in Figure 8. It follows that the entrance effect explains the slight increase of Nu for tubes 1 and 3 when $500 < \mathrm{Re} < 2000$ but does not account for the strong drop of the Nusselt number at low Reynolds numbers.

In order to explain this behavior, the wall and fluid temperatures are plotted against the z coordinate in both the laminar and turbulent regimes. In Figure 10, the wall and fluid temperatures of tube 4 are reported for Re = 380 in the laminar regime, and in Figure 11, they are reported for Re = 4004 in the turbulent regime. In addition, in Figure 12, the local Nusselt

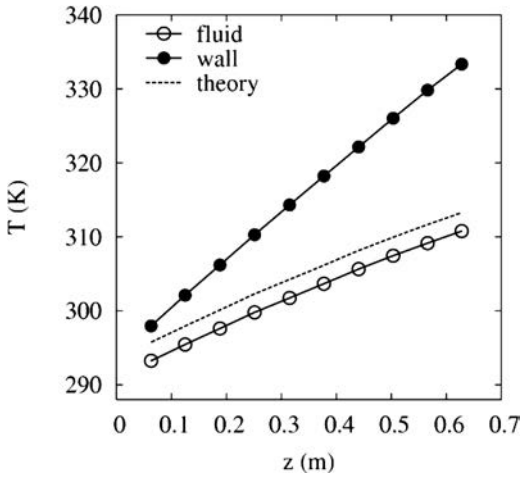

Figure 10 Wall and fluid temperature profile, Re = 380 (tube 4); uncertainties are in Table 3.

number is plotted against the local Reynolds number. As expected for constant heat flux heating, the two profiles are parallel for Re = 4004 (Figure 11) so that the ten local Nusselt numbers are constant along the test section (Figure 12). On the contrary, for Re = 380, the two profiles are divergent (Figure 10), and the ten local Nusselt numbers regularly decrease along the test section (Figure 12). The theoretical wall temperature profile (i.e., calculated from the heat transfer coefficient predicted by Shah and London [7]) is also reported in Figure 10, showing that the experimental slope is about twice the theoretical one.

Such an effect can be attributed to longitudinal heat conduction within the channels walls in the *oz* direction, which modifies the wall temperature profile. The Biot number defined as

$$\mathrm{Bi} = \frac{h \cdot L_j}{k_{al}} \tag{27}$$

may be taken as the dimensionless number representative of longitudinal conduction. For example, in the case of tube 4, Bi is

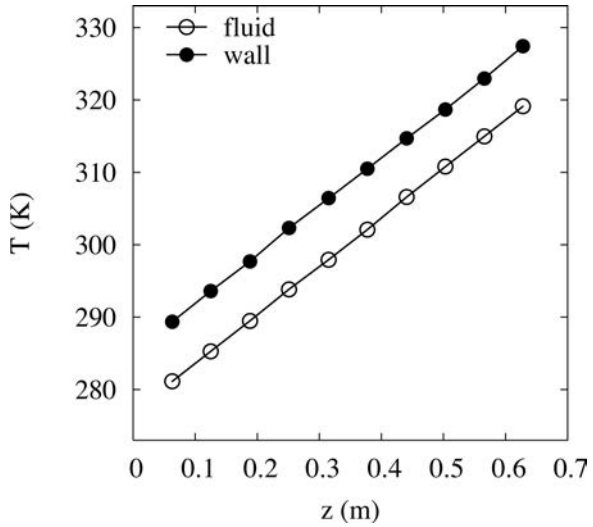

Figure 11 Wall and fluid temperature profile, Re = 4004 (tube 4); uncertainties are in Table 3.

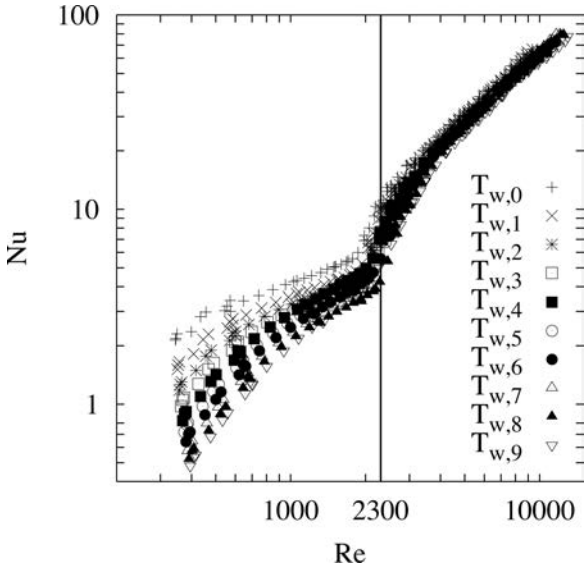

Figure 12 Local Nusselt number versus local Reynolds number (tube 4); uncertainties are in Table 3.

about 1.6 in the laminar regime, so that conductive and convective effects compete to determine the wall temperature profile. On the contrary, Bi is about 14 in the turbulent regime, so that only convective heat transfer drives the wall temperature profile.

Furthermore, despite the high temperature gradient in the z direction (up to 67 K/m), as the aluminium cross-section of the flat tube is small, the longitudinal heat transfer rate

$$\dot{Q}_z = k_{al} \cdot \frac{T_{w9} - T_{w,0}}{z_9 - z_0} \cdot A_{al} \tag{28}$$

is very small. In other words, a small imposed longitudinal heat transfer rate (e.g., heat leaks via external connections) will induce a high temperature gradient because of this small cross-section. This observation leads to important consequences, as shown in Table 6, where two data sets are examined and experimental values are compared to predictions from Shah and London [7]. For tube 4, with as little as a 0.1 W change in the longitudinal heat transfer rate (that is, 2% of thermal leaks or 0.4% of the injected power), the average Nusselt number is overpredicted by a factor of 4.1. The conclusion is not less surprising in the case of tube 1, for which a 0.04 W change in the longitudinal heat transfer rate (that is, 4% of thermal leaks or 0.06% of the injected power) causes the average Nusselt number to be overpredicted by a factor of 1.5. As a consequence, even with a negligible longitudinal heat transfer rate, one can find average Nusselt numbers increasing with the Reynolds number in the laminar regime because of longitudinal conduction. It appears that in small-scale experiments, the data analysis must be revised. Equation (20) is no longer valid because it only takes into account the transversal heat conduction flux, and the internal wall temperature can no longer be assumed to be equal to the measured external wall temperature.

However, because the Nusselt numbers for tubes 1 and 3 when $500 < \mathrm{Re} < 2000$ agree with Shah and London [7] predictions,

Table 6 The longitudinal conduction: comparison of tubes 1 and 4

	Tube 1, Re = 280		Tube 4, Re = 380	
$V \cdot I$ (W)	64		26	
$\dot{Q}_{leak}$ (W)	1		4	
Nu_{Shah}/Nu_{exp}	1.5		4.1	
	Measured	Theory	Measured	Theory
Nu_0/Nu_9	1.2	1	3.8	1
$T_{w,9} - T_{w,0}$ (K)	33	30	40	18
$\dot{Q}_z$ (W)	−0.47	−0.43	−0.2	−0.1

it is felt that heat transfer is not so different in macro- and mini-channels in the laminar regime, and that Nusselt numbers independent of Re should be obtained in mini-channels in the absence of any longitudinal conduction.

Furthermore, a closer look at Table 2 shows that tubes 1,3 and tubes 2,4, of which the Nusselt numbers follow the same trend, have almost equal aluminium cross-section areas. Equation (28) shows that this is not a coincidence. For a given $\dot{Q}_z$, $T_{w,9} - T_{w,0}$ is inversely proportional to A_{al}, all other parameters being equal. Thus, increasing A_{al} for a given wall thickness reduces longitudinal conduction influence, but in doing so, the heat transfer area is increased so that one must also increase the injected power in order to keep the heat flux constant. Not doing so would reduce the wall to fluid temperature difference to the point that uncertainties would become unacceptable. This is not a trivial problem, as a higher injected power means an increased outlet temperature and a higher working pressure to keep the fluid subcooled at the outlet.

THE LAMINAR–TURBULENT TRANSITION

The transition between the two regimes was found to be conveniently characterized by plotting the uncertainties on the wall temperatures against the Reynolds number (see Figure 13). The uncertainty on T_w is

$$\Delta T_w = \sqrt{\Delta T_{cal}^2 + (2\sigma)^2}, \tag{29}$$

ΔT_{cal} being the calibration error and σ the standard deviation calculated from each group of twenty measurements so that 2σ is a statistical uncertainty. Figure 13 exhibits an important peak of uncertainty for $2000 < \mathrm{Re} < 4000$, and ΔT_w is multiplied by ten at its maximum for $\mathrm{Re} \approx 2700$. The following interpretation is proposed. When the transition toward the turbulent regime begins at $\mathrm{Re} > 2000$, at a fixed position along the tube, the flow will periodically become turbulent, and then fall back to the laminar regime. This causes a periodic shift of the heat transfer coefficient and consequently of the wall temperature, which finally increases the statistical uncertainty on the wall temperature. At mid transition ΔT_w is maximum (the flow is supposed to be turbulent half of the time) before decreasing as the turbulence prevails. Then, when the flow is finally always turbulent for $\mathrm{Re} > 4000$, the same value as in the laminar regime is reached with no more heat transfer coefficient fluctuations.

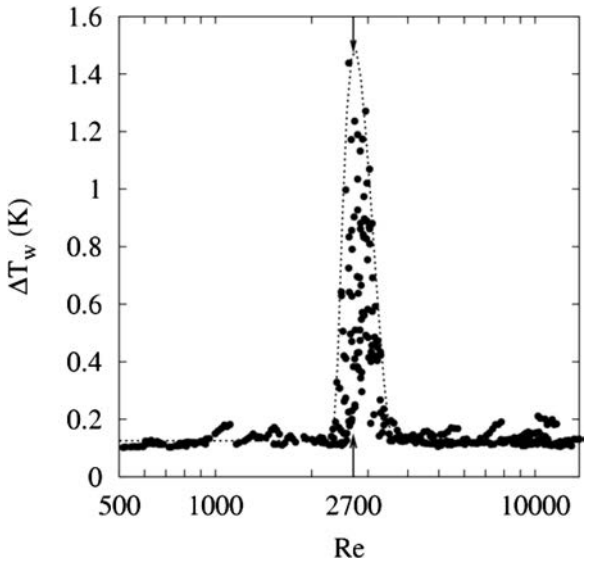

Figure 13 Wall temperatures uncertainties versus Re (tube 3); uncertainties are in Table 3.

CONCLUSIONS

Frictional pressure loss and heat transfer in mini-channels were experimentally investigated. It was emphasized that three phenomena were likely to explain differences reported between mini-channels and macro-tubes. First, one must note that very precise dimensions measurements (i.e., better than ±1%) are essential when dealing with rectangular mini-channels because of the high sensitivity of $4f$ and Nu on geometrical uncertainties.

Second, singular pressure losses were shown to affect the determination of the friction factor in a significant way. Fortunately, these are easy to take into account, and it was demonstrated that with a simple correction, good agreement was found most of the time with friction factors in macro-tubes.

Third, accurate dimension measurements were sufficient to obtain very good agreement between the Gnielinski [12] correlation and our experimental heat transfer results in the turbulent regime. However no accurate prediction was found in the laminar regime. The Ghajar and Tam [13] correlation gave the best prediction but was still unsatisfactory. Thanks to local temperature measurements, it was shown that this discrepancy is probably due to longitudinal conduction. The transversal one-dimensional conduction assumption seems to be no longer valid in mini-channels because these have thick walls compared to their hydraulic diameter. In particular, the convective effects between the internal wall and the fluid, and the conductive effects in the mass of the aluminium, become uncoupled at low Reynolds numbers. Then, extremely small longitudinal heat transfer rates (that is, rates that are negligible compared to the heat flux toward the fluid) can modify the external wall temperature profile so that the Nusselt number calculated with the one-dimensional assumption is greatly overpredicted by classical correlations in the laminar regime. Unfortunately, the very smallness of this longitudinal heat transfer rate prevents any correction on the temperature

measurements, and close examination of Figure 1 shows that experimentally determined laminar Nusselt numbers in mini-channels are still far from macro-tubes results. Thus, new experimental methods should be invented to obtain expected constant Nusselt numbers in the laminar regime for mini-channels.

NOMENCLATURE

a	constant in Eq. (11)
A_{al}	aluminium cross-section area, m^2
A_f	total wetted area, m^2
A_j	heat transfer area, m^2
A_Φ	manifolds flow area, m^2
b	constant in Eq. (11)
Bi	Biot number ($= h \cdot L/k$)
c_p	specific heat capacity, J/kg K
D_h	hydraulic diameter, m
e	wall thickness, m
f	friction factor, see Eq. (1)
G	mass velocity, kg/m^{2}s
g	gravity acceleration, m/s^2
Gr	Grashof number (= Ra/Pr)
h	heat transfer coefficient, W/m^{2}K
I	current, A
k	thermal conductivity, W/m K
L	test section length, m
L_j	heated length, m
l_1	channel width, m
l_2	channel height, m
$\dot{M}$	mass flow rate, kg/s
N	number of channels
Nu	Nusselt number ($= h \cdot D_h/k$)
p	pressure, Pa
P_f	total wetted perimeter, m^2
Δp	pressure loss, Pa
Pr	Prandtl number ($= \mu \cdot c_p/k$)
$\dot{q}$	heat flux, W/m^2
$\dot{Q}_{leak}$	thermal leaks rate, W
$\dot{q}_{leak}$	thermal leaks flux, W/m^2
Q	longitudinal heat transfer rate, W
R_a	tube roughness, m
Ra	Rayleigh number, $(g \cdot \beta \cdot \rho^2 \cdot c_p \cdot D_h^3 \cdot (T_w - T_f))/(\mu \cdot k)$
Re	Reynolds number ($=G \cdot D_h/\mu$)
S_f	fluid flow area, m^2
T	temperature, K
$\Delta T_{sub,in}$	inlet subcooling ($=T_{f,in} - T_{sat}$), K
V	voltage, V
W	flat tube width, m
x,y,z	x,y,z coordinates, m

Greek Symbols

β	cubic thermal expansion coefficient, K^{-1}
γ	aspect ratio (l_2/l_1)
μ	dynamic viscosity, Pa $\cdot$ s
ω	power density, W/m^3
ρ	mass density, kg/m^3
σ	temperature standard deviation, K
ξ	singular pressure loss coefficient

Subscripts

al	aluminium
cal	calibration
cr	critical
exp	experimental
ext	external wall
f	fluid
fr	friction
in	inlet
int	internal wall
k	thermocouple number
l	liquid
out	outlet
sat	saturated
Shah	from Shah and London [7]
sing	singular
sub	subcooled
th	thermal entry length
w	wall
x,y,z	relative to axes *ox,oy,oz*

Superscripts

—	average

REFERENCES

[1] Agostini, B., Watel, B., Bontemps, A., and Thonon, B., Friction Factor and Heat Transfer Coefficient of R134a Liquid Flow in Mini-channels, *Applied Thermal Engineering*, vol. 22, no. 16, pp. 1821–1834, 2003.

[2] Owhaib, W., and Palm, B., Experimental Investigation of Single-Phase Convective Heat Transfer in Circular Microchannels, *Proc. International Symposium on Compact Heat Exchangers, Compact Heat Exchangers, A Festschrift on the 60th Birthday of Ramesh K. Shah,* Grenoble, France, vol. 2, pp. 104–105.

[3] Guo, Z., and Li, Z., Size Effect on Microscale Flow and Heat Transfer, *Heat Transfer 2002*, *Proc. 12th International Heat Transfer Conference*, Grenoble, France, vol. 1, pp. 15–26, Aug. 2002.

[4] Kline, S., and McClintock, F., Describing Uncertainties in Single-Sample Experiments, *Mechanical Engineering*, pp. 3–8, Jan. 1953.

[5] Moffat, R., Contributions to the Theory of Single-sample Uncertainty Analysis, *Journal of Fluids Engineering*, vol. 104, pp. 250–261, 1982.

[6] Moffat, R., Using Uncertainty Analysis in the Planning of an Experiment, *Journal of Fluids Engineering*, vol. 107, pp. 173–182, 1985.

[7] Shah, R., and London, A., *Laminar Flow Forced Convection in Ducts*, Academic Press, London, 1978.

[8] Incropera, F., and DeWitt, D., *Fundamentals of Heat and Mass Transfer*, 4th ed., John Wiley and Sons, New York, 1994.

[9] Tam, L. M., and Ghajar, A. J., Effect of Inlet Geometry and Heating on the Fully Developed Friction Factor in the Transition Region of a Horizontal Tube, *Experimental Thermal and Fluid Science*, vol. 15, pp. 15–52, 1997.

[10] Agostini, B., Étude Expérimentale de l'Ébullition en Convection Forcée de Fluide Réfrigérant dans des Mini-Canaux, Ph.D. thesis, University Joseph Fourier, Grenoble, France, 2002.

[11] Ghajar, A. J., and Tam, L. M., Flow Regime Map for a Horizontal Pipe with Uniform Wall Heat Flux and Three Inlet Configurations, *Experimental Thermal and Fluid Science*, vol. 10, pp. 287–297, 1995.

[12] Gnielinski, V., New Equations for Heat and Mass Transfer in Turbulent Pipe and Channel Flow, *International Chemical Engineering*, vol. 16, no. 2, pp. 359–368, 1976.

[13] Ghajar, A. J., and Tam, L. M., Heat Transfer Measurements and Correlations in the Transition Region for a Circular Tube with Three Different Inlet Configurations, *Experimental Thermal and Fluid Science*, vol. 8, pp. 79–90, 1994.

[14] Adams, T., Abdel-Khalik, S., Jeter, S., and Qureshi, Z., An Experimental Investigation of Single-Phase Forced Convection in Microchannels, *International Journal of Heat and Mass Transfer*, vol. 41, no. 6–7, pp. 851–857, 1998.

[15] Choi, S., and Barron, R., Fluid Flow and Heat Transfer in Micro Tubes, *Micro Mechanical Sensors, Actuators and Systems*, vol. 32, pp. 123–134, 1991.

[16] Garimella, S., Dowling, W., Veen, M. V. D., and Killion, J., The Effect of Simultaneously Developing Flow on Heat Transfer in Rectangular Tubes, *Heat Transfer Engineering*, vol. 22, no. 6, pp. 12–25, 2001.

[17] Taine, J., and Petit, J. P., *Transfers Thermiques*, Dunod, Paris, 1989.

[18] Peng, X., Peterson, G., and Wang, B., Heat Transfer Characteristics of Water Flowing through Microchannels, *Experimental Heat Transfer*, vol. 7, pp. 265–283, 1994.

[19] Wang, B., and Peng, X., Experimental Investigation on Liquid Forced-convection Heat Transfer through Microchannels, *International Journal of Heat and Mass Transfer*, vol. 37, pp. 73–82, 1994.

[20] Peng, X., and Peterson, G., The Effect of Thermofluid and Geometrical Parameters on Convection of Liquids through Rectangular Microchannels, *International Journal of Heat and Mass Transfer*, vol. 38, no. 4, pp. 755–758, 1995.

[21] Peng, X., and Peterson, G., Forced Convection Heat Transfer of Single-phase Binary Mixtures through Microchannels, *Experimental Thermal and Fluid Science*, vol. 12, pp. 99–104, 1996.

[22] Yang, C., and Webb, R., Condensation of R12 in Small Hydraulic Diameter Extruded Aluminium Tubes with and without Micro-Fins, *International Journal of Heat and Mass Transfer*, vol. 39, no. 4, pp. 791–800, 1996.

[23] Harms, T., Kazmierczak, M., and Gerner, F., Developing Convective Heat Transfer in Deep Rectangular Microchannels, *International Journal of Heat and Fluid Flow*, vol. 20, pp. 149–157, 1999.

[24] Mala, G. M., and Li, D., Flow Characteristic of Water in Microtubes, *International Journal of Heat and Fluid Flow*, vol. 20, pp. 142–148, 1999.

[25] Yan, Y., and Lin, T., Condensation Heat Transfer and Pressure Drop of Refrigerant R134a in a Small Pipe, *International Journal of Heat and Mass Transfer*, vol. 42, pp. 697–708, 1999.

[26] Hegab, H., Bari, A., and Ameel, T., Experimental Investigation of Flow and Heat Transfer Characteristics of R-134a in Microchannels, *Microfluidics in BioMEMS*, *Proc. SPIE,* vol. 4560, pp. 117–125, 2001.

[27] Celata, G., Cumo, M., Guglielmi, M., and Zummo, G., Experimental Investigation of Hydraulic and Single-phase Heat Transfer in 0.130 mm Capillary Tube, *Microscale Thermophysical Engineering*, vol. 6, pp. 85–97, 2002.

[28] Agostini, B., Watel, B., Bontemps, A., and Thonon, B., Experimental Study of Single-Phase Flow Friction Factor and Heat Transfer Coefficient in Mini-Channels, *Proc. International Symposium on Compact Heat Exchangers, Compact Heat Exchangers, A Festschrift on the 60th Birthday of Ramesh K. Shah,* Grenoble, France, pp. 85–90, Aug. 2002.